

**Anomalous electrical conduction in a monatomic Pb layer on Ge(111)**

Shinichiro Hatta,\* Takashi Noma, Hiroshi Okuyama, and Tetsuya Aruga†

*Department of Chemistry, Graduate School of Science, Kyoto University, Kyoto 606-8502, Japan*

(Received 5 June 2014; revised manuscript received 12 November 2014; published 3 December 2014)

We studied electrical transport through a Pb monolayer on Ge(111), which has a metallic surface state with a large Rashba spin splitting. The Pb monolayer was found to be metallic down to 9 K. The macroscopic sheet conductivity was  $10.2 \pm 1.0$  mS/□ at 9 K, which is much higher than those of other metallic monolayers. We found that the microscopic step conductivity is two orders of magnitude larger than those in other metallic monolayers, being the main cause of the high macroscopic conductivity. The transport electron-phonon ( $e$ -ph) coupling constant obtained by a temperature-dependent conductance measurement is  $0.16 \pm 0.03$ , indicating weak  $e$ -ph coupling compared to bulk Pb (1.1–1.5). This result is supported by temperature-dependent angle-resolved photoelectron spectroscopy.

DOI: [10.1103/PhysRevB.90.245407](https://doi.org/10.1103/PhysRevB.90.245407)

PACS number(s): 73.20.At, 71.70.Ej

**I. INTRODUCTION**

In the early 20th century, metallic conduction “gave a starting impetus to the modern theory of solids” [1]. Recent development in the physics of nanoscale materials such as graphene [2] and carbon nanotubes [3] has shed a new light on this issue. The metallic conduction in ultrathin metal films on semiconductor surfaces has also been the subject of interest since the pioneering work in 1964 [4]. Recently, mono- or diatomic layers of indium and lead fabricated on silicon surfaces have been found to be metallic down to low temperatures [5], and even superconducting [6–8], where the Peierls instability [9] and Anderson localization [10] tend strongly to destroy the metallicity in low dimensions.

In this paper, we report on our experimental study of electrical transport in a monatomic lead layer formed on a Ge(111) surface, Pb/Ge(111)- $\beta(\sqrt{3} \times \sqrt{3})R30^\circ$  [hereafter denoted Pb- $\beta\sqrt{3}/\text{Ge}(111)$ ]. The Pb- $\beta\sqrt{3}/\text{Ge}(111)$  monolayer is associated with nearly-free-electron-like metallic bands with a spin splitting as large as 200 meV at the Fermi level ( $E_F$ ) due to a giant Rashba spin-orbit interaction (SOI) [11]. We found that the monolayer shows an unexpectedly high electrical conductivity of 10 mS/□, which is an order of magnitude larger than those ever observed in ultrathin metallic films fabricated on semiconductor surfaces. The measurement with a vicinal substrate reveals particularly high step conductivity, which contributes much to the high conductivity at the macroscopic scale. The electron-phonon ( $e$ -ph) coupling was found to be significantly weaker than that in bulk Pb and ultrathin Pb films on Si(111). The high step conductivity, the weak  $e$ -ph coupling, and the large Rashba spin splitting distinguish this surface as a benchmark system to study the electrical and spin transport in two dimensions (2D).

**II. EXPERIMENT**

The Pb- $\beta\sqrt{3}$  monolayer was prepared on Ge(111) substrates ( $n$  type, 10–25  $\Omega$  cm) with a dimension of  $10 \times 3.5 \times 0.5$  mm<sup>3</sup> as prescribed elsewhere [13,14]. The atomic

structure of Pb- $\beta\sqrt{3}/\text{Ge}(111)$  is shown in Fig. 1(a) [12]. The 2D spin-split surface states of Pb- $\beta\sqrt{3}/\text{Ge}(111)$  form a pair of concentric, hexagonal Fermi surfaces ( $ss_1$  and  $ss_2$ ) as schematically shown in Fig. 1(b). Although a small Fermi surface due to the subsurface 2D state ( $ss_{\text{sub}}$ ) is present near  $\bar{\Gamma}$  [15] as schematically shown in Fig. 1(b), the contribution of the subsurface state to electrical conduction should be only a few percent of that of the Pb-derived surface states because of a much smaller Fermi contour and group velocity.

Conductance measurements were carried out by using a home-built four-point-probe (4PP) system with a probe distance of 1 mm. The probes are attached *in vacuo* to the sample after the sample preparation. Stable, high-precision variable-temperature measurements are realized by carefully prepared probe-sample contact with thermal drift suppressed [16]. As the temperature was increased or decreased at a rate of 1–2 K/min,  $I$ - $V$  curves were recorded successively. An Ohmic  $I$ - $V$  characteristic with linear slope  $R$  was obtained at  $-5 \mu\text{A} \leq I \leq 5 \mu\text{A}$  over the whole temperature range studied, 9–350 K. The sheet resistivity  $\rho$  was obtained as the product of the resistance  $R$  and the geometrical correction factor  $F = 4.2$ , the latter being calculated from the layout of the probe electrodes and the sample size [17]. The angle-resolved photoelectron spectroscopy (ARPES) measurements were done with a hemispherical electron energy analyzer and He  $I_\alpha$  radiation ( $h\nu = 21.22$  eV). The angle and energy resolutions were  $0.3^\circ$  and 10 meV, respectively.

**III. RESULTS AND DISCUSSION**

In order to determine precisely the electrical conductivity of the Pb- $\beta\sqrt{3}$  monolayer, the contribution of the Ge substrate to the conduction should be minimized. In order to quantify the contribution of the substrate, we first measured the temperature dependence of the resistivity for Bi/Ge(111)- $(\sqrt{3} \times \sqrt{3})R30^\circ$ , whose electronic structure is known to be semiconducting [18]. The resistivity for Bi/Ge(111) shown in Fig. 2 exhibits the temperature dependence characteristic of bulk Ge. The rapid resistivity decrease with increasing  $T$  at  $T < 80$  K is due to thermal carrier generation from the donor level. After the saturation regime at 80–250 K, the resistivity again decreases steeply. The fitting of  $\sigma = \sigma_0 \exp[-E_g/(2k_B T)]$  to the high-temperature regime gives  $E_g = 0.67$  eV (the inset in Fig. 2),

\*hatta@kuchem.kyoto-u.ac.jp

†aruga@kuchem.kyoto-u.ac.jp

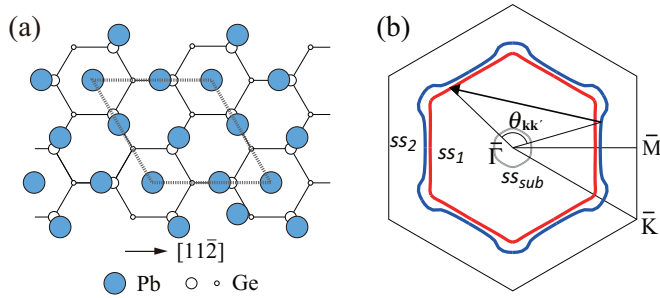


FIG. 1. (Color online) (a) Atomic structure of Pb/Ge(111)- $\beta(\sqrt{3} \times \sqrt{3})R30^\circ$  [12]. The fractional coverage of Pb is  $4/3$ . (b) Schematic Fermi contours of surface states. Outer most hexagon represents the surface  $(\sqrt{3} \times \sqrt{3})$  Brillouin zone.

which agrees with the bulk band gap of Ge. The increase of the resistivity with  $T$  seen in the intermediate temperature range is due to thermal enhancement of  $e$ -ph scattering rate in the saturation regime. Thus it is clear that the resistivity of Bi/Ge(111) represents that of the Ge(111) substrate.

We measured the resistivity of Pb- $\beta\sqrt{3}$ /Ge(111), which is also shown in Fig. 2. The resistivity measured at low temperatures for Pb- $\beta\sqrt{3}$ /Ge(111) is much lower than that for Bi/Ge(111). It monotonically increases with temperature up to  $\sim 290$  K, which indicates the metallic conduction in Pb- $\beta\sqrt{3}$ . On semiconductor substrates, the adsorbate-induced carrier accumulation in the space-charge layer is suggested to make a contribution to the electrical conductance [19,20]. In the present case, however, the resistivity of Pb- $\beta\sqrt{3}$  approaches asymptotically that of Bi/Ge(111) at  $T > 320$  K, which indicates that the conductivity through a space-charge layer

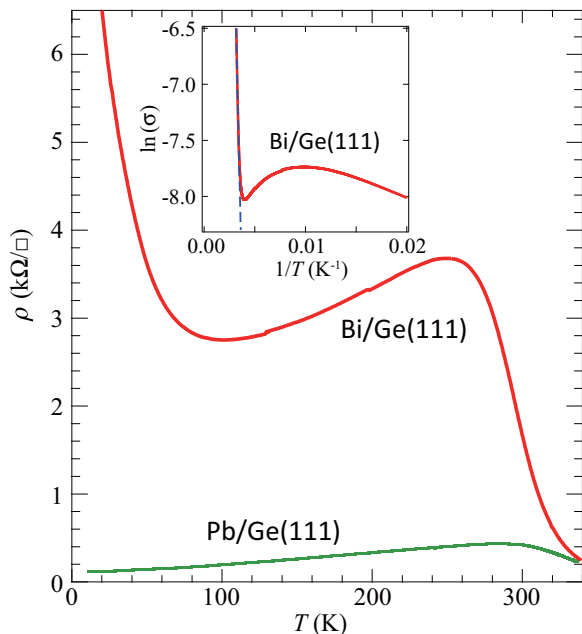


FIG. 2. (Color online) Temperature dependence of the sheet resistivity of Bi/Ge(111) and Pb- $\beta\sqrt{3}$ /Ge(111). The inset shows the  $\ln(\sigma)$ - $1/T$  plot for Bi/Ge(111). Dashed line shows  $\sigma \propto \exp[-E_g/(2k_B T)]$  with  $E_g = 0.67$  eV.

of the Ge substrate is negligible ( $< 0.05$  mS/ $\square$ ), even at 300 K. Note that the contribution of the space-charge layer should decrease with temperature. Thus the measured conductivity is represented by the sum of the surface-state conductivity  $\sigma_{ss}$  and the bulk conductivity. The bulk contribution is reduced to below 3% at  $T \leq 60$  K.

It is worth noting here that the measured temperature dependence of the sheet resistivity does not show any sign of a transition down to 9 K. This is consistent with the scanning tunneling microscopy (STM) observation at 6 K [21]. The almost-straight sides of the hexagonal Fermi surfaces [Fig. 1(b)] appear to satisfy the Fermi contour nesting condition and may lead to an insulating charge-density-wave phase at low temperatures. However, in the present case, the Fermi contour sections at  $\pm \mathbf{k}_F$  have opposite spin polarization due to Rashba SOI, which prohibits the nesting and protects the metallic behavior down to very low temperatures.

The resistivity of Pb- $\beta\sqrt{3}$  prepared on three different, nominally flat Ge(111) substrates are shown in Fig. 3(a). A linear, metallic temperature dependence is seen for all the samples. The sample-dependent variation of  $\sigma_{ss}$  is attributed to the difference in the density of surface defects such as atomic steps and contamination. It is found that the gradient becomes moderate below  $\sim 25$  K. The resistivity at 9 K must be close to the residual resistivity. The measured minimum resistivities on the flat substrates correspond to the sheet conductivity of  $\sigma_{ss} = 10.2 \pm 1.0$  mS/ $\square$ .

In Fig. 3(c), the conductivity of Pb- $\beta\sqrt{3}$ /Ge(111) is compared with those of Pb films epitaxially grown on Si(111) [22,23]. Note that Pb/Ge(111) is not suitable to study the conductivity of thicker Pb films because of the high conductivity of the first Pb- $\beta\sqrt{3}$  monolayer which is formed

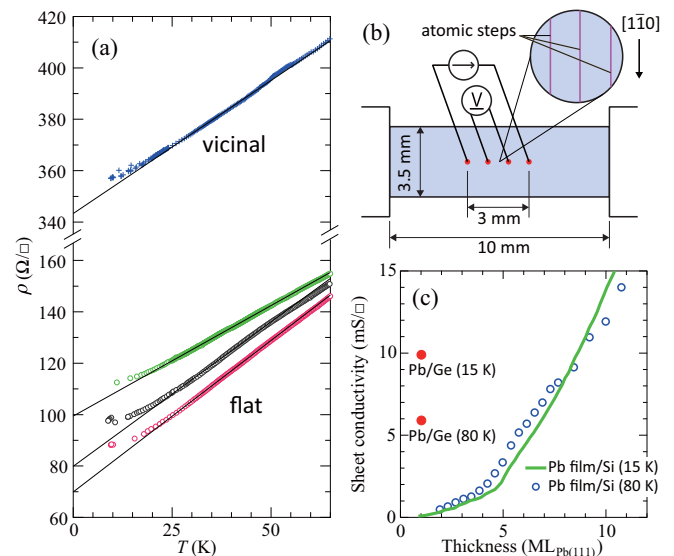


FIG. 3. (Color online) (a) Temperature dependence of the resistivity of Pb- $\beta\sqrt{3}$  on three nominally flat Ge(111) substrates and a vicinal one. Solid lines represent the linear fit to the data at  $T > 25$  K. (b) Schematic of the arrangement of 4PP measurement. (c) Comparison of the sheet conductivity of Pb- $\beta\sqrt{3}$ /Ge(111) (solid circles) with those of Pb films epitaxially grown on Si(111)- $(7 \times 7)$  (solid line) [22] and Pb/Si(111)- $(\sqrt{3} \times \sqrt{3})R30^\circ$  (open circles) [23].

TABLE I. Comparison of transport and electronic properties of ultrathin metallic films.

Surfaces	$\sigma$ [mS/ $\square$ ]	$\sigma_{\text{step}}$ [S/m]	$k_F$ [ $\text{\AA}^{-1}$ ]	$v_F$ [ $10^8$ cm/s]	$d\rho/dT$ [ $\Omega/\text{K}$ ]	$\lambda_{\text{tr}}$	Ref.
Ge(111) $\beta(\sqrt{3} \times \sqrt{3})$ -Pb	10.2 (9 K)	$8 \times 10^5$	0.36, 0.39	1.13, 0.90	1.0	$0.16 \pm 0.03$	This work, [13]
Si(111) $(\sqrt{7} \times \sqrt{3})$ -In	2.44 (5 K)	$3 \times 10^3$	1.4	1.47	0.8	1.2	[5,7,24]
Si(111) $(\sqrt{3} \times \sqrt{3})$ -Ag	0.075 (RT)	$5 \times 10^3$	0.10	0.89			[25,26]

upon Pb deposition without annealing. On the other hand, the conductivity of the Pb films on Si appears to decrease to a very low value with decreasing thickness, indicating that the interfacial layer is insulating. Surprisingly, the conductivity of the Pb- $\beta\sqrt{3}$  monolayer is comparable to that of the films of 8 or 9 layers thick, even though the electron transport in a monolayer should be more strongly altered by surface defects such as steps. Since the wave function of the metallic surface state on the Pb- $\beta\sqrt{3}$ /Ge(111) surface is confined in the Pb- $\beta\sqrt{3}$  monolayer [14], the observed high electrical conductivity may indicate the peculiarity of the Pb- $\beta\sqrt{3}$  monolayer.

In Table I, we compare the transport and electronic properties of Pb- $\beta\sqrt{3}$ /Ge(111) with those of ultrathin In and Ag films on Si(111). In/Si(111)- $(\sqrt{7} \times \sqrt{3})$  has an In bilayer [27] and Ag/Si(111)- $(\sqrt{3} \times \sqrt{3})$  has a Ag monolayer on top of Si(111). Each surface has a 2D free-electron-like surface-state band. From among the three surfaces, Ag/Si(111) has a lower conductivity due mostly to the small Fermi contour. On the other hand, the In/Si(111)- $(\sqrt{7} \times \sqrt{3})$  surface has the largest Fermi wave vector ( $k_F$ ) among the three surfaces, which would result in electrical conductivity more than an order of magnitude larger than that of Pb- $\beta\sqrt{3}$ . However, the measured conductivity of Pb- $\beta\sqrt{3}$  is much larger than that of In/Si(111)- $(\sqrt{7} \times \sqrt{3})$ .

Note that the difference in macroscopic conductivity does not necessarily reveal the intrinsic properties of the surfaces, since the macroscopic conductivity should be strongly affected by surface steps and their density should be different for different surfaces. In order to gain insight into the intrinsic transport property of the Pb- $\beta\sqrt{3}$ /Ge surface, let us discuss below the step conductivity  $\sigma_{\text{step}}$ .

In order to determine the step conductivity, we prepared a Pb- $\beta\sqrt{3}$  monolayer on a vicinal Ge(111) substrate whose surface normal was nominally tilted by  $2.5^\circ$  from [111] toward  $[\bar{1}\bar{1}2]$ . Figure 4(a) shows the low-energy electron diffraction (LEED) pattern from Pb- $\beta\sqrt{3}$  formed on the vicinal substrate. The step-induced satellite spots are seen around the (01) spot. Four satellite peaks were confirmed in the line profile along the  $[\bar{1}\bar{1}2]$  (horizontal) direction, as shown in Fig. 4(b). The distance between the satellite peaks gave the mean terrace width of 5.2 nm, which is in reasonable agreement with that expected for the surface with bilayer-height steps and the nominal miscut angle. The array of 4PP was set perpendicular to the steps [Fig. 3(b)].

The measured sheet resistivity of the vicinal Pb- $\beta\sqrt{3}$  surface is shown in Fig. 3(a). The resistivity at 9 K was higher by  $\sim 250 \Omega/\square$  than that on the nominally flat substrates. On the other hand, for the temperature dependence, there is negligible difference between the flat and vicinal substrates, as expected from the Matthiessen's rule, indicating that different scattering processes contribute to the resistivity independently. If there

are  $N_{\text{step}}$  steps between two voltage probes, the resistivity due to the steps is given by  $FN_{\text{step}}R_{\text{step}} = FN_{\text{step}}/(l\sigma_{\text{step}})$ , where  $R_{\text{step}}$  denotes the resistance of a monatomic step and  $l$  is the step length through which the current passes [25]. In the present case,  $l$  equals the width of the sample, 3.5 mm. The density of steps on the vicinal substrate is  $n_1 = 1/5.2 \text{ nm}^{-1}$ . On the nominally flat substrate, the step density is estimated to be  $n_2 = 1/30 \text{ nm}^{-1}$ . The resistivity increase on the vicinal substrate is then given by  $Fd(n_1 - n_2)/(l\sigma_{\text{step}})$ , where  $d = 1 \text{ nm}$  denotes the distance between the two voltage probes. Thus we obtain  $\sigma_{\text{step}} = 8 \times 10^5 \text{ S/m}$ . This is significantly higher than  $3 \times 10^3 \text{ S/m}$  for In/Si(111)- $(\sqrt{7} \times \sqrt{3})$  [7] and  $5 \times 10^3 \text{ S/m}$  for Ag/Si(111)- $(\sqrt{3} \times \sqrt{3})$  [25].

The above result clearly indicates that the high macroscopic conductivity of the Pb- $\beta\sqrt{3}$  surface is due, partly, to the high step conductivity. On the other hand, by using the values of  $\sigma_{\text{step}}$  and  $n_2$ , the contribution of the steps to the sheet resistivity of the nominally flat surface is estimated to be  $Fdn_2/(l\sigma_{\text{step}}) \sim 55 \Omega/\square$ . It is likely that the step resistance dominates the residual resistance of the Pb- $\beta\sqrt{3}$  monolayer, which suggests that the sheet conductivity of a step-free Pb- $\beta\sqrt{3}$  monolayer should be even higher than that observed above.

Next, let us estimate the relaxation time and the mean-free path of conducting electrons on Pb- $\beta\sqrt{3}$ . The 2D conductivity based on the Boltzmann equation for nondegenerate states is given as

$$\sigma_{2D} = \frac{e^2\tau}{4\pi^2\hbar} \int \frac{v_{kx}^2}{|v_k|} dk, \quad (1)$$

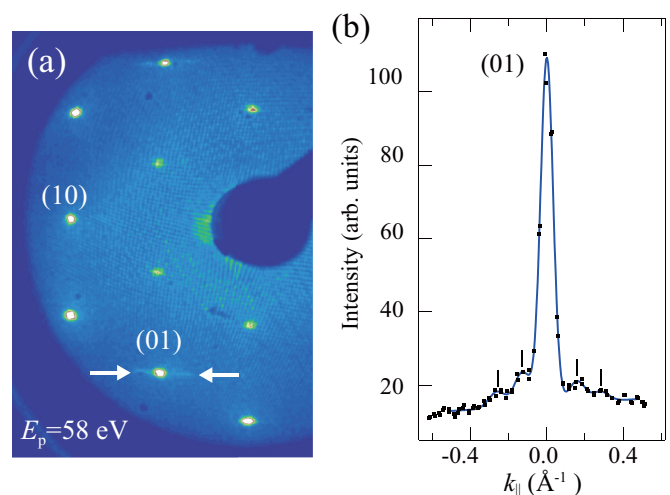


FIG. 4. (Color online) (a) LEED pattern of Pb- $\beta\sqrt{3}$  formed on vicinal Ge(111). (b) A line profile along a line between the arrows in (a).

where  $v_k$  is the group velocity,  $\nabla_k \epsilon(k)/\hbar$ , and the integral is done on Fermi contours in a surface Brillouin zone. Here a  $k$ -independent relaxation time  $\tau$  is assumed. The band structure measured along  $\bar{\Gamma}\bar{K}$  and  $\bar{\Gamma}\bar{M}$  by ARPES was used to evaluate the group velocity. We performed numerical integrations for  $ss_1$  and  $ss_2$ , taking the  $\bar{\Gamma}\bar{M}$  direction as the  $x$  axis, which is parallel to the array of 4PP. We obtained the relaxation time of 77 fs at 9 K. By using the Fermi velocity (Table I) averaged for  $ss_1$  and  $ss_2$ ,  $1.0 \times 10^8$  cm/s, the mean-free path was estimated to be 77 nm. The mean-free path is comparable to, or larger than, the terrace size on the nominally flat Ge(111) substrate, which indicates that the scattering rate is quite low within a terrace.

In order to gain further insight into the microscopic transport property of  $\text{Pb-}\beta\sqrt{3}$ , let us concentrate now on the  $e$ -ph scattering. The strength of the  $e$ -ph scattering is described by the  $e$ -ph coupling constant  $\lambda$ . For surface-state conduction,  $\lambda$  is often determined by the temperature dependence of the surface-state lineshape observed by ARPES. On the other hand, the temperature dependence of the resistivity is described by the transport  $e$ -ph coupling constant  $\lambda_{\text{tr}}$ , which is given by  $\lambda_{\text{tr}} = \langle (1 - \cos \theta_{\mathbf{k}\mathbf{k}'}) |\langle \mathbf{S}_{\mathbf{k}} | \mathbf{S}_{\mathbf{k}'} \rangle|^2 \rangle \lambda$ , where  $\theta_{\mathbf{k}\mathbf{k}'}$  denotes the scattering angle [Fig. 1(b)]; the factor of  $1 - \cos \theta_{\mathbf{k}\mathbf{k}'}$  is maximum at  $\theta_{\mathbf{k}\mathbf{k}'} = \pi$  (backscattering) [28,29]. If the scattering probability  $|\langle \mathbf{S}_{\mathbf{k}} | \mathbf{S}_{\mathbf{k}'} \rangle|^2$  is independent of  $\theta_{\mathbf{k}\mathbf{k}'}$ ,  $\lambda_{\text{tr}}$  equals  $\lambda$ . In the present case, there are the two concentric Fermi surfaces with the opposite spin polarization, which enables electrons to be backscattered without the spin-flip process. Therefore, it is expected that  $\lambda_{\text{tr}}$  agrees with  $\lambda$ .

We now determine  $\lambda_{\text{tr}}$  from the linear temperature dependence of the measured sheet resistivity. According to the Bloch–Grüneisen theory of metallic conduction, the linear temperature dependence of  $\rho$  is seen above  $T \sim \Theta_D/3$ . Since the linear temperature dependence appears above 25 K in Fig. 3(a),  $\Theta_D$  is estimated at  $\sim 80$  K. This is consistent with that determined by a dynamical LEED analysis [12]. In the high-temperature regime, the phonon scattering rate  $1/\tau_{\text{ph}}$  is represented by  $2\pi\lambda_{\text{tr}}k_B T/\hbar$ . Since the temperature dependence of  $\rho$  is governed by phonon scattering, we obtained  $\lambda_{\text{tr}} = 0.16 \pm 0.03$  from  $d\rho/dT = 1.0 \pm 0.15 \Omega/\text{K}$  by assuming a common  $\tau_{\text{ph}}$  for  $ss_1$  and  $ss_2$ .

The transport  $e$ -ph coupling constant  $\lambda_{\text{tr}}$  of  $\text{Pb-}\beta\sqrt{3}$  is significantly smaller than  $\lambda$  determined for bulk Pb ( $\lambda = 1.1$  to 1.5), Pb quantum-well films on Si(111) (0.7–1.0) [30] and a Pb monolayer on Si(111) (1.07) [6]. Except for  $\lambda$  in bulk Pb, these values were evaluated from the temperature-dependent ARPES measurements of quantum-well states or a surface state.

In order to verify the marked difference in the magnitude of  $\lambda$ , we used ARPES which is a tool to investigate state-specific  $\lambda$ . Here,  $\lambda$  at  $E_F$  is important in relation to electrical conductance. In order to determine  $\lambda$ , we used the relation  $\lambda = (d\Delta E/dT)/(2\pi k_B)$ , where  $\Delta E$  is the ARPES peak width in energy. The temperature dependence of  $\Delta E$  is dominated by the  $e$ -ph interaction at temperatures higher than  $\Theta_D$  and, thus,  $\Delta E$  should decrease linearly with temperature. The ARPES intensity maps measured at different temperatures are shown in Fig. 5(b). The narrowing of the surface-state band width is clearly seen in the whole energy range shown here. In order to avoid the influence of the Fermi distribution

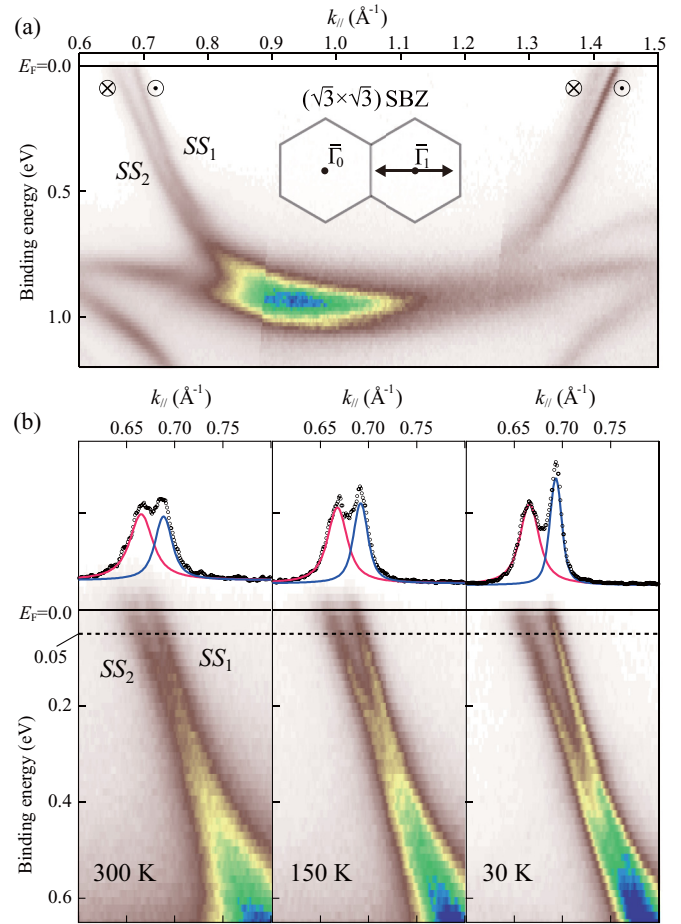


FIG. 5. (Color online) (a) The ARPES intensity map for  $\text{Pb-}\beta\sqrt{3}/\text{Ge}(111)$  measured along  $\bar{\Gamma}\bar{M}$  at 30 K. The inset indicates the  $(\sqrt{3} \times \sqrt{3})$  surface Brillouin zones and the  $k_{\parallel}$  region displayed. The markers ( $\otimes$  and  $\odot$ ) indicate the in-plane spin polarization direction. (b) High-resolution ARPES images (bottom) of the spin-split surface states at 300, 150, and 30 K. The upper panels show MDC (dots) at 50 mV below  $E_F$  and two Voigt curves (red and blue lines) fit to the MDC.

function, we first extracted the momentum distribution curves (MDC) and evaluated the width  $\Delta k$  which is defined as the Lorentzian width of the Voigt function fit to the MDC [see upper panels of Fig. 5(b)]. The temperature dependencies of  $\Delta k$  at several binding energies are shown in Fig. 6(a). Second,  $\Delta E$  was obtained as the product of  $\Delta k$  with the gradient of the dispersion,  $d\epsilon(k)/dk$ , at each binding energy. Finally  $\lambda$  was determined from a linear fit to the  $\Delta E - T$  data between 90 and 300 K. Note that the temperature range was chosen so that  $T > \Theta_D = 80$  K. The result is given in Fig. 6(b).

At a binding energy of 200 meV,  $\lambda$  for  $ss_1$  is  $\sim 1$  and that for  $ss_2$  is  $\sim 0.45$ . As the energy approaches  $E_F$ ,  $\lambda$  of each band becomes smaller. The energy dependence of  $\lambda$  can be discussed in terms of the electron density of states participating the hole relaxation [31]. Since the bulk valence band maximum on the  $\text{Pb-}\beta\sqrt{3}/\text{Ge}(111)$  surface is located at 0.05–0.1 eV below  $E_F$  [13,15], the bulk density of states starts to increase at this binding energy, which is consistent with the observed energy dependence of  $\lambda$ . The  $\lambda$  value at binding energies below

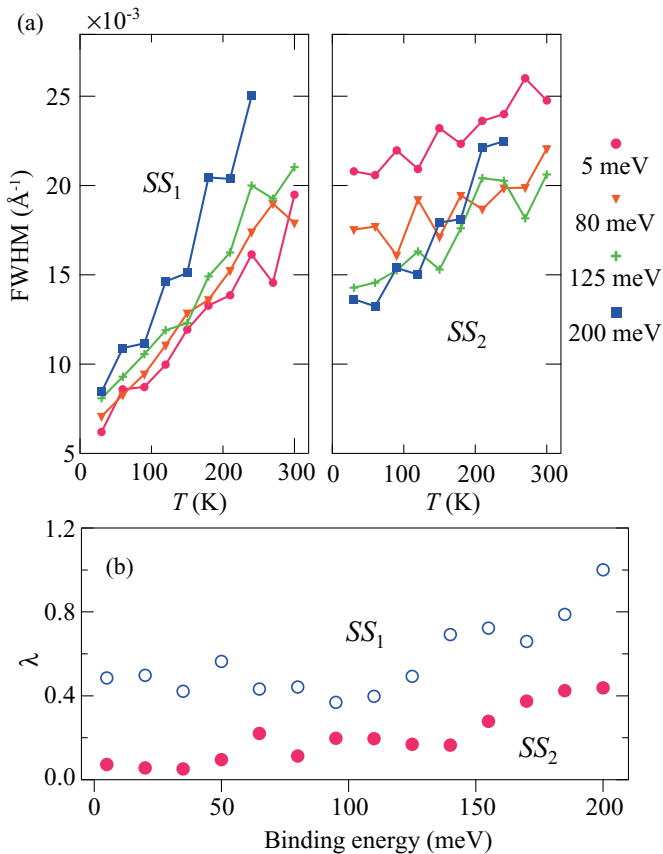


FIG. 6. (Color online) (a) Temperature dependencies of  $\Delta k$  (FWHM) of  $ss_1$  (left) and  $ss_2$  (right) at binding energies of 5, 80, 125, and 200 meV. (b)  $\lambda$  of each spin-split surface state as a function of binding energy.

40 meV was averaged, which yielded  $0.47 \pm 0.10$  for  $ss_1$  and  $0.06_{-0.06}^{+0.10}$  for  $ss_2$ .

The origin of the difference in  $\lambda$  for  $ss_1$  and  $ss_2$  is not obvious. The ARPES intensity map at 30 K shown in Fig. 5(a) shows that, while the  $ss_1$  branch is sharper at the left-hand side, the  $ss_2$  branch is sharper at the right-hand side. As a result, the relative magnitude of  $\lambda$  for  $ss_1$  and  $ss_2$  is switched at the right-hand side. A similar phenomenon was observed for spin-split surface bands on Sb(111) [32]. This suggests that the difference in  $\lambda$  may not be intrinsic to the initial states but is probably due to an extrinsic effect such as the photoemission final-state effect. In any case, the magnitude of  $\lambda$  determined here is significantly smaller than that for bulk Pb or other Pb films, which does not contradict the result obtained for  $\lambda_{tr}$ . However, it is difficult, based only on this result, to confirm  $\lambda = \lambda_{tr}$ .

Note that the magnitude of  $\lambda$  can also be evaluated by the analysis of the band renormalization derived from the  $e$ -ph interaction. The renormalization is observed by ARPES as a kink in band dispersion at low binding energies comparable to a typical phonon energy  $\hbar\omega_D$ . However, this method is difficult to apply to a system with weak  $e$ -ph coupling and low  $\hbar\omega_D$  as in the present case. The value of  $\hbar\omega_D$  on Pb- $\beta\sqrt{3}$  is estimated to be 7 meV using  $\Theta_D = 80$  K and  $\hbar\omega_D = k_B\Theta_D$ . It is difficult to recognize a kink at such a low binding

energy in the surface-state band structure shown in Figs. 5(a) and 5(b).

The unexpectedly high sheet conductivity  $\sigma$  of  $\beta$ -Pb/Ge(111) as compared with In/Si(111) and Ag/Si(111) should be, in part, due to the difference in the density of surface defects such as steps, which is known to depend on the sample and preparation conditions. On the other hand, the step conductivity  $\sigma_{step}$  should be less affected by extrinsic factors and hence can be considered more as a material-specific property. The high step conductivity should be ascribed to a higher transmission probability for electrons at steps, which may be due to a lower potential barrier at steps for conduction electrons. STM must be a promising tool to study the mechanism of electron scattering at steps and to clarify a key factor of the anomalous electrical conductivity.

Let us finally remark on the possibility of the superconductivity in Pb- $\beta\sqrt{3}$ /Ge(111). The present result indicates that the  $e$ -ph coupling is much weaker in Pb- $\beta\sqrt{3}$  than in bulk Pb or in other Pb films. According to the strong-coupling theory [33], the superconducting transition in Pb- $\beta\sqrt{3}$ /Ge(111) is expected to occur at a temperature significantly lower than  $T_c = 7.2$  K in bulk Pb. Because the surface state on Pb- $\beta\sqrt{3}$  is strongly localized in the Pb monolayer, 2D surface phonon modes must play a dominant role in the  $e$ -ph coupling. The surface-atom density of Pb- $\beta\sqrt{3}$  is higher than that of Pb(111) by 2%, which would lead to higher energies of LA phonon modes. This partially explains the weaker  $e$ -ph coupling of Pb- $\beta\sqrt{3}$ . Our result suggests that  $\lambda$  determined by ARPES may be affected by extrinsic effects, which indicates  $\lambda_{tr}$  obtained from the electrical transport measurement is more appropriate for the discussion of superconductivity.

In conclusion, we have shown that Pb- $\beta\sqrt{3}$ /Ge(111) is metallic down to 9 K, at which temperature the sheet conductivity in a macroscopic scale as well as the step conductivity of the monolayer is much higher than those of the previously known ultrathin metallic films. Another anomaly found for this surface is that the  $e$ -ph coupling constant is an order of magnitude smaller than that of bulk Pb and Pb films. These results demonstrate that the electrical transport in a monolayer, even in a classical regime, cannot be predicted by the extrapolation of the bulk or thicker-film properties. Finally, let us point out that this surface should serve as a benchmark system to study 2D transport phenomena, such as spin accumulation, magnetotransport, and the Kondo effect in a Rashba spin system. One can easily introduce various scatterers, such as atoms, molecules, and overlayers, at various concentrations on top of the Pb- $\beta\sqrt{3}$  monolayer. Thus the monolayer provides a broad opportunity to study the interplay between 2D electrons with large Rashba SOI with various scatterers, which may be magnetic or nonmagnetic, with scattering potentials of short or long range, etc., and will contribute to the exploration of 2D electronic transport.

#### ACKNOWLEDGMENTS

The present work was financially supported by JSPS KAKENHI (Grant No. 24340069).

- [1] N. W. Ashcroft and N. D. Mermin, *Solid State Physics* (Harcourt, Fort Worth, 1976), p. 2.
- [2] K. S. Novoselov, A. K. Geim, S. V. Morozov, D. Jiang, M. I. Katsnelson, I. V. Grigorieva, S. V. Dubonos, and A. A. Firsov, *Nature (London)* **438**, 197 (2005).
- [3] A. Thess, R. Lee, P. Nikolaev, H. J. Dai, P. Petit, J. Robert, C. H. Xu, Y. H. Lee, S. G. Kim, A. G. Rinzler, D. T. Colbert, G. E. Scuseria, D. Tomanek, J. E. Fischer, and R. E. Smalley, *Science* **273**, 483 (1996).
- [4] P. J. Estrup and J. Morrison, *Surf. Sci.* **2**, 465 (1964).
- [5] S. Yamazaki, Y. Hosomura, I. Matsuda, R. Hobara, T. Eguchi, Y. Hasegawa, and S. Hasegawa, *Phys. Rev. Lett.* **106**, 116802 (2011).
- [6] T. Zhang, P. Cheng, W.-J. Li, Y.-J. Sun, G. Wang, X.-G. Zhu, K. He, L. Wang, X. Ma, X. Chen, Y. Wang, Y. Liu, H.-Q. Lin, J.-F. Jia, and Q.-K. Xue, *Nat. Phys.* **6**, 104 (2010).
- [7] T. Uchihashi, P. Mishra, M. Aono, and T. Nakayama, *Phys. Rev. Lett.* **107**, 207001 (2011).
- [8] M. Yamada, T. Hirahara, and S. Hasegawa, *Phys. Rev. Lett.* **110**, 237001 (2013).
- [9] G. Grüner, *Density Waves in Solids* (Addison Wesley, Massachusetts, 1994).
- [10] P. W. Anderson, *Phys. Rev.* **109**, 1492 (1958).
- [11] É. I. Rashba, *Fizika tverd. tela* **2**, 1224 (1960) [*Sov. Phys. Solid State* **2**, 1109 (1960)]; Yu. A. Bychkov and É. I. Rashba, *Pis'ma v ZhETF* **39**, 66 (1984) [*JETP Lett.* **39**, 78 (1984)].
- [12] Y. Ohtsubo, H. Muto, K. Yaji, S. Hatta, H. Okuyama, and T. Aruga, *J. Phys.: Condens. Matter* **23**, 435001 (2011).
- [13] K. Yaji, Y. Ohtsubo, S. Hatta, H. Okuyama, K. Miyamoto, T. Okuda, A. Kimura, H. Namatame, M. Taniguchi, and T. Aruga, *Nat. Commun.* **1**, 17 (2010).
- [14] K. Yaji, S. Hatta, T. Aruga, and H. Okuyama, *Phys. Rev. B* **86**, 235317 (2012).
- [15] K. Yaji, Y. Ohtsubo, S. Hatta, H. Okuyama, R. Yukawa, I. Matsuda, P. L. Fevre, F. Bertran, A. Taleb-Ibrahimi, A. Kakizaki, and T. Aruga, *J. Electron Spectrosc. Relat. Phenom.* (to be published).
- [16] S. Hatta, H. Okuyama, and T. Aruga (unpublished).
- [17] M. Yamashita and M. Agu, *Jpn. J. Appl. Phys. (1962–1981)* **23**, 1499 (1984).
- [18] S. Hatta, T. Aruga, Y. Ohtsubo, and H. Okuyama, *Phys. Rev. B* **80**, 113309 (2009).
- [19] S. Hasegawa and S. Ino, *Phys. Rev. Lett.* **68**, 1192 (1992).
- [20] S. Hasegawa, X. Tong, S. Takeda, N. Sato, and T. Nagao, *Prog. Surf. Sci.* **60**, 89 (1999).
- [21] H. Morikawa, I. Matsuda, and S. Hasegawa, *Phys. Rev. B* **77**, 193310 (2008).
- [22] O. Pfennigstorf, A. Petkova, H. L. Guenter, and M. Henzler, *Phys. Rev. B* **65**, 045412 (2002).
- [23] N. Miyata, K. Horikoshi, T. Hirahara, S. Hasegawa, C. M. Wei, and I. Matsuda, *Phys. Rev. B* **78**, 245405 (2008).
- [24] Eli Rotenberg, H. Koh, K. Rossnagel, H. W. Yeom, J. Schäfer, B. Krenzer, M. P. Rocha, and S. D. Kevan, *Phys. Rev. Lett.* **91**, 246404 (2003).
- [25] I. Matsuda, M. Ueno, T. Hirahara, R. Hobara, H. Morikawa, C. Liu, and S. Hasegawa, *Phys. Rev. Lett.* **93**, 236801 (2004).
- [26] I. Matsuda and S. Hasegawa, *J. Phys.: Condens. Matter* **19**, 355007 (2007).
- [27] J. W. Park and M. H. Kang, *Phys. Rev. Lett.* **109**, 166102 (2012).
- [28] G. D. Mahan, *Many-Particle Physics*, 3rd ed. (Kluwer Academic/Plenum, New York, 2000).
- [29] G. Grimvall, *The Electron-Phonon Interaction in Metals* (North-Holland, Amsterdam, 1981).
- [30] Y. F. Zhang, J. F. Jia, T. Z. Han, Z. Tang, Q. T. Shen, Y. Guo, Z. Q. Qiu, and Q. K. Xue, *Phys. Rev. Lett.* **95**, 096802 (2005).
- [31] J. E. Gayone, S. V. Hoffmann, Z. Li, and Ph. Hofmann, *Phys. Rev. Lett.* **91**, 127601 (2003).
- [32] Z.-J. Xie *et al.*, *Chin. Phys. Lett.* **31**, 067305 (2014).
- [33] W. L. McMillan, *Phys. Rev.* **167**, 331 (1968).